IEEE Access
Multidisciplinary | Rapid Review | Open Access Journal

Received March 13, 2020, accepted March 29, 2020, date of publication April 13, 2020, date of current version April 29, 2020.

Digital Object Identifier 10.1109/ACCESS.2020.2987196

Unambiguous Reconstruction for Multichannel Nonuniform Sampling SAR Signal Based on Image Fusion

LIMING ZHOU, XIAOLING ZHANG, (Member, IEEE), YANGYANG WANG, LIANG LI, LIMING PU, JUN SHI, (Member, IEEE), AND SHUNJUN WEI, (Member, IEEE)

School of Information and Communication Engineering, University of Electronic Science and Technology of China, Chengdu 611731, China

Corresponding author: Xiaoling Zhang (xlzhang@uestc.edu.cn)

This work was supported in part by the National Key Research and Development Program of China under Grant 2017YFB0502700, in part by the High Resolution Earth Observation Youth Foundation under Grant GFZX04061502, and in part by the National Natural Science Foundation of China under Grant 61671113, Grant 61501098, and Grant 61571099.

ABSTRACT Multichannel signal processing in azimuth is a vital technique to enable a wide-swath Synthetic Aperture Radar (SAR) with high azimuth resolution. However, the multichannel high-resolution and wide-swath (HRWS) SAR system always suffers from the problem of the azimuth nonuniform sampling resulting in the image ambiguity, when it does not satisfy the uniform sampling condition. In this paper, to suppress the azimuth image ambiguity, we propose a novel unambiguous reconstruction method based on image fusion. During this reconstruction processing, the Back Projection (BP) algorithm is first utilized for SAR imaging to obtain the designed sub-images. Then, the reconstruction expression is derived as the summation of the sub-images weighted by the interpolation coefficient. This method integrates the reconstruction into the imaging process and the image fusion makes the procedure simple. In addition, the interpolation period, which affects the reconstruction image quality and efficiency, is further analyzed. Moreover, as the curved trajectory platform brings more challenges for the unambiguous reconstruction, the performance of the proposed method applied to the curved trajectory platform is studied. Finally, experimental results clearly verify the effectiveness of the proposed method for ambiguity suppression and demonstrate its applicability to the curved trajectory.

INDEX TERMS High resolution and wide swath, nonuniform sampling, signal reconstruction, synthetic aperture radar (SAR).

I. INTRODUCTION

With the further research on the Synthetic Aperture Radar (SAR) imaging technology, high resolution and wide swath (HRWS) imaging has become an important trend for the future Earth observation [1]–[4]. For the conventional SAR system, to obtain a wide swath image, low pulse repetition frequency (PRF) is required to avoid the serious range ambiguity. Meanwhile, the PRF must be high enough to guarantee the azimuth sampling frequency satisfying the wide Doppler Bandwidth and then avoid azimuth ambiguity. The multichannel technique is served as a potential solution to this contradiction [5]–[10]. The multichannel SAR system transmits the signals with low PRF to ensure a wide-range swath and receives the signals of all channels simultaneously. If the multichannel uniform sampling condition is strictly met [5], [11], the multichannel raw data can be combined, which equals to the raw data collected by a single-channel SAR system with high sampling frequency. As the equivalent sampling frequency of the multichannel SAR system increases in azimuth, it ensures that the azimuth large bandwidth signal is unambiguous for achieving high azimuth resolution. To strictly meet the uniform sampling condition, the antenna spacing, the platform velocity, and the PRF must be fixed. However, the equivalent antenna spacing may change with the platform attitude variation during

The associate editor coordinating the review of this manuscript and approving it for publication was Jinming Wen.

the movement, while the maneuverable or satellite platform velocity is not constant either. Besides, an increased PRF is required for improved azimuth ambiguity suppression in some case. Therefore, these deviations from the fixed parameters result in the multichannel SAR system typically dissatisfying the uniform sampling condition. The raw data obtained by the multichannel is nonuniformly sampled in azimuth, leading to the azimuth ambiguity. As a result, unambiguous reconstruction becomes a critical problem for the nonuniform sampling multichannel SAR signal processing.

Since the image ambiguity is essentially caused by nonuniform sampling, a large number of articles have studied the signal reconstruction problem to obtain the uniform sampling signals. To suppress the ambiguity, Krieger *et al.* developed the filter bank reconstruction (FBA) algorithm [5], and the influence of this algorithm on the signal-to-noise ratio (SNR) and azimuth ambiguity is analyzed [6]. However, the performance of this unambiguous reconstruction may not be optimal when there appears noise [12]. To increase the robustness of the reconstruction algorithm, an adaptive reconstruction method based on the space-time adaptive processing (STAP) approach [7], [13] and its modifications [12], [14], [15] are proposed, which extract the desired spectrum components from the space-time plane by means of space-time beamforming to obtain the unambiguous full spectrum. These methods are adaptive under practical working conditions. Nevertheless, when the correlation of the Doppler aliasing component is strong, the performance of these methods is greatly attenuated.

In addition, there are several other kinds of unambiguous reconstruction algorithms which can suppress the ambiguity well, such as the spectrum reconstruction method and the interpolation reconstruction method [16]–[18]. For the spectrum reconstruction, Liu *et al.* show that the spectrum of the uniformly sampled signal can be recovered in the frequency domain [16]. Due to the Nonuniform Discrete Fourier Transform (NUDFT) used to transfer the nonuniform sampling signal, the spectrum reconstruction algorithm suffers from heavy computation. To improve efficiency, some modified spectrum reconstruction methods based on Nonuniform Fast Fourier Transform (NUFFT) are presented [11], [19], [20]. Moreover, as the Fractional Fourier Transform (FrFT) has been proved as a perfect tool to improve the reconstruction quality [21], [22], a nonuniform sampling signal spectrum reconstruction based on FrFT is proposed for formation-flying satellites SAR [17]. Above methods have to transform the raw data into the frequency domain, while the interpolation reconstruction method can directly process the raw data in the time domain. An interpolation reconstruction algorithm (IRA) is discussed to recover the unambiguous signal for Small Satellite MultiChannel SAR [18], which employs the generalized sampling theorems [23]. However, the spectrum reconstruction methods and the interpolation reconstruction method are non-adaptive, which are sensitive to channel amplitude-phase error, strong noise and array position error. Additionally, these algorithms first reconstruct the raw data to obtain uniformly sampled data and then use frequency domain imaging algorithms, such as Range-Doppler algorithm and Omega-K algorithm, for SAR imaging. Therefore, these algorithms perform poorly when applied to the curved trajectory reconstruction.

In this situation, we innovatively propose an image domain reconstruction method (IDR) to solve the unambiguous reconstruction problem for a multichannel SAR system. During the reconstruction, firstly the back projection (BP) algorithm [24]–[27] is employed for SAR imaging to get the sub-images. Since the BP algorithm doing coherent accumulation to obtain each pixel's value in the imaging scene, it facilitates the image fusion after imaging of each channel. Then, the sub-images are weighted by the interpolation coefficient which is generated by the interpolation formula [23] to recover the unambiguous image. Compared with the conventional reconstruction methods processed in the data domain, the proposed method provides a new viewpoint in the image domain to solve the unambiguous reconstruction problem. From this point of view, the expression of the image domain method is very concise, which is a form of weighted summation of the sub-images.

The main contributions of our work are as follows:

1. When there is an equivalent antenna spacing error, the reconstruction result needs to be updated. The proposed method can simply implement the update only by re-calculating the correct interpolation coefficient and fusing the sub-image, which avoids the process of re-imaging.

2. Due to the combination of the reconstruction and the back projection strategy, the proposed method can solve the problem of the curved trajectory SAR reconstruction.

The rest of this paper is organized as follows. In section II, the general signal model of the multichannel SAR is introduced. The reconstruction for periodic nonuniform sampling signal is reviewed in section III and an image domain reconstruction algorithm is proposed with detailed derivations. In section IV, the experimental results of simulated multichannel data and artificial multichannel data generated from single channel SAR verify the effectiveness of the proposed image domain processing method. Finally, section V provides some conclusions.

II. SIGNAL MODEL FOR MULTICHANNEL SAR SYSTEM

As the multichannel technology is utilized to achieve HRWS SAR imaging, this section first describes the geometry model and sampling mode for the multichannel HRWS SAR system in azimuth. Then, the authors analyze the echo characteristics of the multichannel system and discuss the interpolation period in details.

A. GEOMETRY AND MULTICHANNEL SAMPLING MODEL

The geometric model of the multichannel SAR system is depicted in Fig.1, where the y-axis is the direction of platform movement. In order to achieve the HRWS SAR imaging, multiple channels are uniformly distributed in the along-track dimension, where one of the channels transmits the signal and

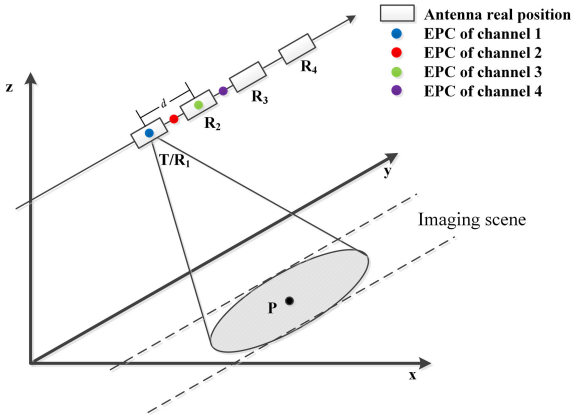

FIGURE 1. Geometric mode for multichannel SAR system.

all of the channels simultaneously receive the echo signal. Since the range between the platform and the observed scene is much larger than the spacing of the channels, each channel can be considered to illuminate the same area in the same beam direction. In Fig.1, a four-channels SAR system is taken as an example. T/R_1 is the transceiver regarded as a reference channel which translates and receives the signal with a broad beam in range direction. R_2, R_3 and R_4 are the rest of channels just receiving the echo.

As the multichannel SAR data can be converted into an equivalent monostatic SAR data corresponding to the effective phase centers (EPCs) by compensating constant phase with respect to the reference channel T/R_1 [28], we can analyze the EPCs to study the characteristic of the multichannel SAR sampling. The sampling model of the multichannel SAR system is shown in Fig.2, which contains three pulse repetition intervals. Assuming d is the antenna spacing, the baseline length between the nth antenna and the reference antenna is $x_n = (n-1)\cdot d$, where $n = 1, 2, 3, 4$. The corresponding EPC position of the nth antenna is $epc_n = x_n/2$. In a pulse repetition interval, the baseline interval between two adjacent EPCs is a constant $d/2$. During a pulse repetition period, the moving distance of the antenna is $L = V/PRF$, where V is the platform velocity, PRF is the pulse repetition frequency. In the uniform sampling model, the baseline interval between two adjacent EPCs, adjacent sampling points, should be constant during consecutive pulse repetition intervals. Therefore, the multichannel SAR system should satisfy the uniform sampling condition, which is expressed as

$$\frac{V}{PRF} = N \cdot \frac{d}{2} \tag{1}$$

where N is the number of channels, and $N = 4$ in Fig.2.

However, in practical engineering applications, there are some problems to satisfy the uniform sampling condition shown in (1). A rigid selection of the PRF may be in conflict with the timing diagram for some incident angles [5], and sometimes the PRF needs to be set larger to increase the azimuth sampling frequency for improved azimuth ambiguity suppression. Furthermore, the velocity and the attitude of the platform may change continuously during the movement. Therefore, the uniform sampling condition is difficult to meet. The EPCs of the multichannel SAR system will always be nonuniformly distributed in azimuth, shown in Fig.2, which results in periodic nonuniform sampling in azimuth. This will cause the azimuth image ambiguity. This paper conducts research on the unambiguous reconstruction for the nonuniform sampling signal in the following sections.

B. ECHO MODEL AND INTERPOLATION PERIOD ANALYSIS

Essentially, the azimuth ambiguity suppression is an signal reconstruction problem for the azimuth nonuniform sampling raw data. Therefore, we first analyze the characteristics of raw data of the multichannel SAR system. After the range compression, the echo of the point scatter P_m in the imaging scene can be expressed as

$$s_c(\tau, \eta; P_m) = \alpha(P_m)\, w_a(\eta; P_m) \times \sin c\left\{B\left(\tau - \frac{2R(\eta; P_m)}{c}\right)\right\} \cdot \exp\left\{\frac{-j4\pi R(\eta; P_m)}{\lambda}\right\} \tag{2}$$

where, τ is the fast-time variable, η is the slow time variable, P_m is the m-th point scatter, $\alpha(P_m)$ is the complex-valued reflectivity for the m-th scatterer, $w_a(\eta; P_m)$ is the antenna pattern function, B is the bandwidth, $R(\eta; P_m)$ is the range between the antenna and the m-th scatterer P_m at slow time η.

The echo of the whole scene can be written as

$$s_c(\tau, \eta) = \int_{P_m \in \Omega} s_c(\tau, \eta; P_m)\, dP_m \tag{3}$$

where Ω is imaging scene. Due to the relative motion between the antenna and the scatters in the imaging scene, the distance from the scatters to the antenna at the different slow time is constantly changing. So the two-dimensional SAR echo of the scatters displays coupling phenomenon. At different slow time, the echo of scatters distributed in different range gates terms distance migration.

Normally, interpolation reconstruction method obtains the reconstructed signal by interpolating the nonuniform sampling raw data. However, due to the distance migration problem, the azimuth raw data is distributed in different range gates, making it two-dimensional. The interpolation period determines the number of raw data points used to reconstruct. By appropriately choosing, the effect of coupling can be ignored, which can be derived from the range model.

Assuming that the slow time variable is equal to zero when the motion antenna is closest to the target in the scene, The distance from the antenna to the m-th point scatterer P_m can be expressed as

$$R(\eta; P_m) = \sqrt{R_0^2 + V^2\eta^2} \tag{4}$$

where, R_0 is the shortest distance from P_m to the line trajectory of the antenna and V is the platform velocity.

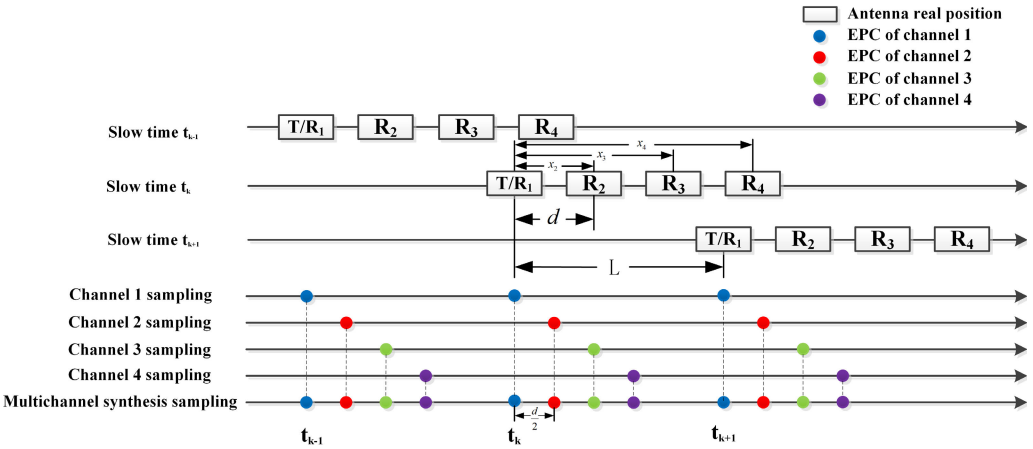

FIGURE 2. Azimuth sampling mode for multichannel SAR system.

For the azimuth time spacing Δt, the distance migration can be expressed as

$$\begin{aligned}\Delta R(\eta, \Delta t; P_m) &= |R(\eta+\Delta t; P_m) - R(\eta; P_m)| \\ &\approx \left| \frac{V^2\eta_c}{R(\eta_c; P_m)}\Delta t + \frac{V^2\cos^2\theta_c}{R(\eta_c; P_m)}(\eta-\eta_c)\Delta t \right|\end{aligned} \tag{5}$$

where η_c is the time when the scatter P_m is illuminated by the beam center, θ_c is the squint angle. Assuming T is the synthetic aperture time, then $\eta_c - \frac{T}{2} \le \eta \le \eta_c + \frac{T}{2}$. If the radar is forward-looking, $\eta_c < 0$. When $\eta = \eta_c - \frac{T}{2}$, the absolute value of the distance migration is maximized.

The echo signal in azimuth can be considered as one dimensional signal, ignoring the effect of the range coupling [18], when the range migration does not exceed one range unit. This condition can be expressed as

$$\Delta R \le \rho \tag{6}$$

where ρ denote the range sampling spacing.

Let $\Delta t = l \cdot \frac{1}{PRF}, l \in \mathbb{N}$, from (5) and (6) the condition of decouple can be expressed as

$$0 \le l \le \left\lfloor \frac{\rho \cdot PRF}{V\sin\theta_c + \frac{V^2\cos^2\theta_c T}{2R(\eta_c; P_m)}} \right\rfloor \tag{7}$$

where, $\lfloor\cdot\rfloor$ means rounding down. It means that within azimuth adjacent l pulse repetition periods, the two-dimensional raw data is not coupled in the rang-direction. In the reconstruction process, the data of several adjacent pulse repetition periods in azimuth is utilized for interpolation reconstruction, and the number of periods is called the interpolation period. Hence, to ignore the effect of the range coupling, the interpolation period must be less than l. A more thoughtful choice for interpolation period concerned with the reconstruction quality and the efficiency of the proposed method is analyzed in the next section.

III. AZIMUTH UNAMBIGUOUS RECONSTRUCTION

In this section, we first review the generalized sampling theorem for the nonuniform sampling signal, where the interpolation coefficient will be used in the proposed method. After that, an unambiguous reconstruction method based on image fusion is proposed.

A. GENERALIZED SAMPLING THEOREM

A bandwidth-limited signal can be uniquely determined by the values of the periodic nonuniform sampling points, which is called as generalized sampling theorem [23]. That is to say, the uniform sampling signal can be reconstructed by the nonuniform sampling data. According to the analysis of the echo signal, the raw data of the multichannel SAR can be regarded as nonuniformly sampled signals in azimuth which satisfy the generalized sampling theorem. For the multichannel SAR system, the sampling time of the k-th nonuniform points for channel n can is given by

$$t_{k,n} = kT_r + t_n \tag{8}$$

where T_r is the sampling period. t_n is the n-th channel sampling time bias which can be written as follows

$$t_n = (n-1)\cdot T_b, \quad n = 1, \cdots, N \tag{9}$$

where T_b is the time interval of the two adjacent equivalent sampling points. N denotes the total channel number. The reconstructed uniform signal is equally distributed along the azimuth direction with a time interval T_r/N. The azimuth time of the uniform sampling points within the k_0-th sampling period, which is used to recover uniform sampling signal for channel i, can be express as

$$\begin{aligned}t = k_0 T_r + \frac{(i-1)T_r}{N} \\ i = 1, \ldots, N, k_0 = 1 + L/2, \ldots, K - L/2\end{aligned} \tag{10}$$

where K is the number of azimuth sampling periods of the raw data. $L \in \mathbb{N}$ is the interpolation period.

So the reconstruction for periodic nonuniform sampling signal can be expressed as

$$s(t) = \sum_{k=k_0-L/2}^{k=k_0+L/2} \sum_{n=1}^{N} s(t_{k,n}) \Psi_{kn}(t) \tag{11}$$

where

$$\Psi_{kn}(t) = \frac{\prod_{q=1}^{N} \sin[\pi PRF(t - t_q)]}{\prod_{\substack{q=1 \\ \neq n}}^{N} \sin[\pi PRF(t_n - t_q)]} \cdot \frac{(-1)^{kN}}{\pi PRF(t - t_{k,n})} \tag{12}$$

The nonuniform sampling signals are weighted by the interpolation coefficient and summed to obtain uniform sampling signals. This interpolation coefficient will be used in the proposed image domain reconstruction method.

The value of L cannot be too large to satisfy the condition of decoupling in range direction, shown in (7). In addition, the reconstruction accuracy increases with the enlarging of the L. However, the increasing of L account for the greater calculation while the excessively enlarging interpolation period has little effect on improving the reconstruction accuracy. This is because the attenuation of the interpolation function $\Psi_{kn}(t)$ value is fast and the contribution of the original signal $s(t_{k,n})$ farther from the interpolation point t to the reconstruction result is smaller. Therefore, considering the interpolation quality and efficiency, the minimum interpolation period which makes the ambiguity value of the reconstructed image less than -60dB is used as the interpolation period.

B. IMAGE DOMAIN RECONSTRUCTION METHOD

In this sub-section, we propose an image domain reconstruction (IDR) method to solve the unambiguous reconstruction problem. Generally, according to the BP algorithm [27], the BP component of the mth pixel of the final image by using the uniform sampling data can be expressed as

$$I(m) = \sum_{k_0=1}^{K} s_r(\tau(t, m), t) \exp\{j\omega\tau(t, m)\} \quad m = 1, 2, \cdots, M \tag{13}$$

where $s_r(\tau(t, m), t)$ is the range compressed echo of the m-th pixel at uniform sampling slow-time t. $\tau(t, m)$ is the dual echo delay from the EPC to the m-th pixel at slow-time t, ω is the center angular frequency of the transmitted signal, M and K are the number of the pixels in the imaging scene and the number of sampling periods respectively.

As the echo of a multichannel system is nonuniformly sampled, the uniform sampling data $s_r(\tau(t, m), t)$ needs to be reconstructed. In addition, since the SAR azimuth signal is weighted by the antenna pattern, the signal in the main lobe of the pattern is approximately considered to be band-limited. We can use the generalized sampling theorem. According to (11), the reconstruction of the uniform sampling data through the interpolation of the N channels raw data in azimuth direction can be shown as

$$s_r(\tau(t, m), t) = \sum_{k=k_0-M/2}^{k=k_0+M/2} \sum_{n=1}^{N} s_r(\tau(t_{k,n}, m), t_{k,n}) \Psi_{kn}(t) \tag{14}$$

s_r is the combined raw signal from each channel's individual signal abiding by the azimuth sampling time sequence. $t_{k,n}$ is the nonuniform sampling time expressed in (8). $s_r(\tau(t_{k,n}, m), t_{k,n})$ is the nonuniform sampling data. According to (10), t is the uniform sampling time of channel i, which is the time of the reconstructed data. $\Psi_{kn}(t)$ is the interpolation coefficient.

Substituting (14) into (13), the reconstruction imaging of channel i can be written as

$$\begin{aligned} I_i(m) &= \sum_{k_0=1+\frac{L}{2}}^{K-\frac{L}{2}} s_r(\tau(t, m), t) \exp\{j\omega\tau(t, m)\} \\ &= \sum_{k_0=1+\frac{L}{2}}^{K-\frac{L}{2}} \sum_{k=k_0-\frac{L}{2}}^{k_0+\frac{L}{2}} \sum_{n=1}^{N} s_r(\tau(t_{k,n}, m), t_{k,n}) \Psi_{kn}(t) \\ &\quad \cdot \exp\{j\omega\tau(t, m)\} \\ m &= 1, 2, \cdots, M \end{aligned} \tag{15}$$

In (12), let $l \in \left[-\frac{L}{2}, \frac{L}{2}\right]$, k can expressed as $k = k_0 + l$. $\Psi_{kn}(t)$ can be rewritten as $\Psi_{ln}(t)$ which depends on the parameter l, channel n and uniform sampling time t. The interpolation coefficient is periodic. When N is even, $\Psi_{kn}(t)=\Psi_{kn}(t+T_r)$, and when N is odd, $\Psi_{kn}(t)=\Psi_{kn}(t+2T_r)$. Assuming the N is even, $\Psi_{ln}(t)$ only depends on parameter l and channel n, which can be written as Ψ_{ln}. When N is odd, there are similar expressions. So (15) can be expressed as

$$\begin{aligned} I_i(m) &= \sum_{l=-\frac{L}{2}}^{\frac{L}{2}} \sum_{n=1}^{N} \sum_{k=1+\frac{L}{2}+l}^{K-\frac{L}{2}+l} s_r(\tau(t_{k,n}, m), t_{k,n}) \\ &\quad \cdot \exp\{j\omega\tau(t, m)\} \Psi_{ln} \\ &= \sum_{l=-L/2}^{L/2} \sum_{n=1}^{N} I_{l,n}(m) \Psi_{ln} \\ m &= 1, 2, \cdots, M \end{aligned} \tag{16}$$

where

$$I_{l,n}(m) = \sum_{k=1+\frac{L}{2}+l}^{K-\frac{L}{2}+l} s_r(\tau(t_{k,n}, m), t_{k,n}) \exp\{j\omega\tau(t, m)\} \tag{17}$$

$I_{l,n}(m)$ is not a SAR imaging result of each channel but an image constructed for reconstruction, which is defined as sub-image. The original raw data corresponding to the nonuniform sampling time $t_{k,n} = (k_0 + l)T_r + t_n$ is projected to sub-image $I_{l,n}(m)$. Correspondingly, the phase history from the EPC to the m-th pixel at the uniform sampling time $t = k_0 T_r + \frac{(i-1)T_r}{N}$ is compensated.

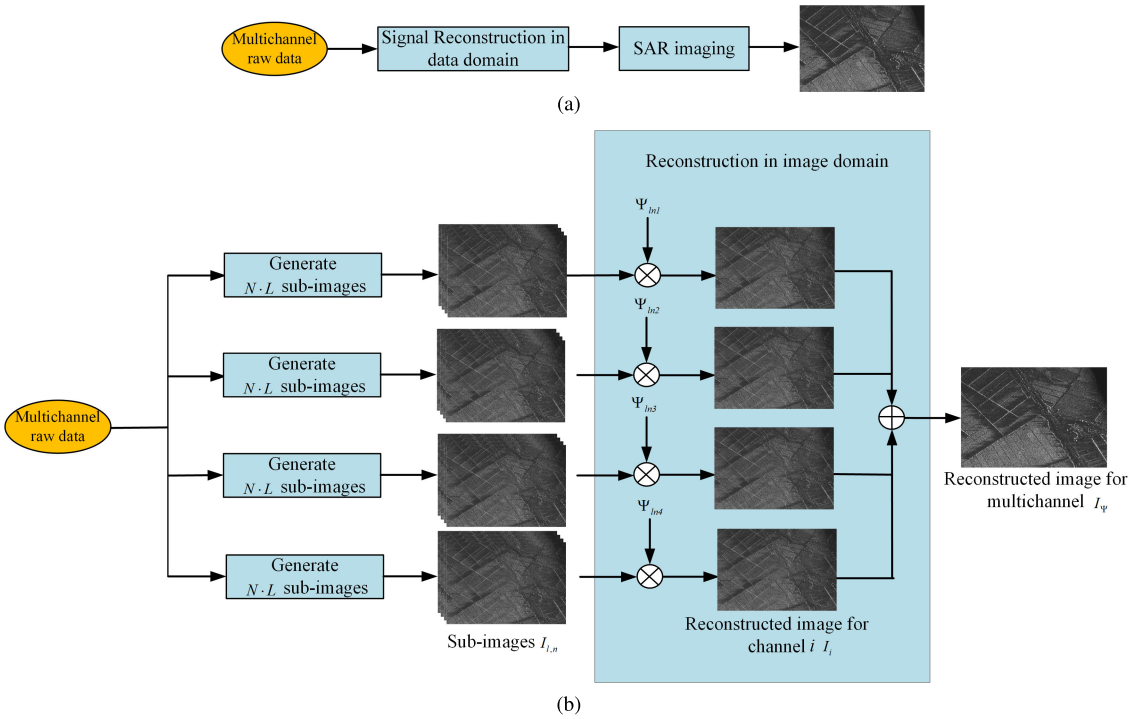

FIGURE 3. Comparison of conventional data domain reconstruction method and the proposed image domain reconstruction method. (a)The conventional method. (b) The image domain reconstruction method.

The imaging results $I_{l,n}$, which are weighted by coefficient Ψ_{ln}, are summed up to get the reconstructed image $I_i(m)$ for channel i. For each channel, this process of reconstruction fuses the sub-images generated from multichannel data in the image domain.

The final imaging result $I_\Psi(m)$ of the unambiguous reconstruction for multichannel nonuniform sampling in azimuth SAR signal is a summation of the N single-channel reconstructed images $I_i(m)$, which can be expressed as

$$I_\Psi(m) = \sum_{i=1}^{N} I_i(m) \tag{18}$$

C. PROPERTY ANALYSIS

In this subsection, we will discuss some properties of the image domain reconstruction method, such as structural characteristics, computational complexity, and ambiguity suppression analysis.

The first issue we are concerned about is to compare the structural characteristics of the traditional method and the proposed method. The first step of the conventional reconstruction method is multichannel raw data reconstruction in the data domain and then the second step uses the reconstructed data to realize the final SAR imaging. Compared with the conventional reconstruction method, the proposed method integrates the reconstruction into the SAR imaging process. The flow of the image domain reconstruction method is depicted in Fig.3(b). The sub-images of each channel are first generated by the multichannel raw data using BP algorithm, preparing for image domain processing. Then, according to the reconstruction formula (12), we can obtain the interpolation coefficient. Finally, the sub-images weighted by the interpolation coefficient are fused in the image domain expressed in (16) and (18). This expression, which is a weighted summation of the images, is simple.

Moreover, when there is an equivalent antenna spacing error, the antenna spacing d is not accurate. The reconstruction process needs to be implemented again for better reconstruction results. The conventional method has to reconstruct the echo data again and then utilize the reconstructed data for SAR imaging. However, only by adjusting the interpolation coefficient, the proposed method can easily obtain the new reconstruction results, which avoids the process of re-imaging. Because the interpolation coefficient, which can be separated, is not related to the sub-imaging results.

The second issue to be addressed is the computational complexity. Assume that the number of range-direction samples of a multichannel SAR system is N_R, the number of azimuth-direction samples for one channel is N_A, and the length and width of the imaging scene are N_x and N_y. Using the echo data of one channel, the computation amount of each step of the BP algorithm can be expressed as:

Step 1 (Range Compression): The frequency-domain compression method is used. This step includes N_A FFT, N_A IFFT, and N_A point-by-point complex multiplication operations. The amount of computation is as follow: $N_A N_R(\log(N_R) + 1)$ complex multiplication and $2N_A N_R \log(N_R)$ complex addition, where $\log(\cdot)$ represents a base-2 logarithm.

Step 2 (Range Data interpolation/ Resampling): Using frequency domain interpolation technique, this step includes

N_A N_R-point FFT, N_A kN_R-point complex multiplication and N_A kN_R-point IFFT. The amount of computation is as follow: $\frac{N_A N_R}{2}\log(N_R)+kN_A N_R+\frac{kN_A N_R}{2}\log(kN_R)$ complex multiplication and $N_A N_R\log(N_R)+kN_A N_R\log(kN_R)$ complex addition, where k is the interpolation multiple.

Step 3 (Calculating the Distance History): This step needs to calculate the distance between the transceiver platform and the scatterer at each slow time. The amount of computation is as follow: $4N_A N_x N_y$ real multiplication, $5N_A N_x N_y$ real addition and $N_A N_x N_y$ Square operation.

Step 4 (Calculating Index): This step needs to calculate the corresponding position of each scatterer in the echo data at each slow moment. The amount of computation is as follow: $N_A N_x N_y$ real multiplication and $N_A N_x N_y$ real addition.

Step 5 (Coherent Accumulation): This step needs to calculate the echo delay phase of each scatterer in the imaging scene at each slow time, and then compensate the phase and coherently accumulate them. The amount of computation is as follow: $N_A N_x N_y$ real multiplication, $N_A N_x N_y$ complex exponential operation, $N_A N_x N_y$ complex multiplication and $N_A N_x N_y$ complex addition.

From the analysis of the calculation amount of each step of the BP algorithm, it can be known that the calculation amount of the BP algorithm is mainly in the back projection part. The time complexity of the algorithm can be expressed as $O(N_A N_x N_y)$. Using one channel echo data for BP imaging, the total amount of calculation can be recorded as Θ_{BP}. Thus, when the proposed image domain reconstruction method is used for reconstruction, the amount of calculation to generate sub-images is $NL\Theta_{BP}$. Then, N sub-images are fused, where the amount of calculation is $NL\cdot N_x N_y$ complex multiplication and $(NL-1)\cdot N_x N_y$ complex addition. When the reconstruction result needs to be adjusted, it is not necessary to perform sub-image imaging again, but only perform fusion process. Its computation amount is $NL\cdot N_x N_y$ complex multiplication and $(NL-1)\cdot N_x N_y$ complex addition, which greatly reduces the calculation amount of updating reconstruction.

The third issue we are concerned about is to further explain the ambiguity suppression in the image domain. Let m_a represent the pixels of an ambiguity component in the imaging result. $\widetilde{I}_i(m_a), i = 1, 2, \cdots, N$ represents the value of the ambiguity component of each channel before reconstruction. The magnitude of the ambiguity components of each channel is the same, and the phase is different. The real parts of the ambiguity components of channel 1 and channel $N/2+1$ are shown in Fig.4. Multichannel imaging results are obtained by accumulating the images of each channel. The multichannel ambiguity value $\widetilde{I}(m_a)$ can be expressed as

$$\widetilde{I}(m_a)=\sum_{i=1}^{N}\widetilde{I}_i(m_a) \tag{19}$$

As the ambiguity value of each channel cannot be offset after accumulation, the final image still suffers from the ambiguity. In order to suppress ambiguity, the phase of the ambiguity value $\widetilde{I}_i(m_a)$ of each channel needs to be adjusted.

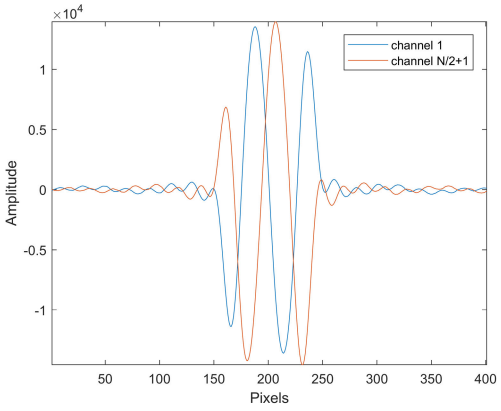

FIGURE 4. Real parts of the ambiguity components before reconstruction.

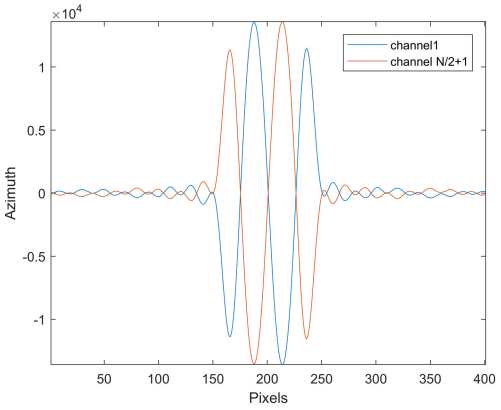

FIGURE 5. Real parts of the ambiguity components after reconstruction.

The ambiguity value $I_i(m_a)$ of each channel after reconstruction is obtained by weighted summing the ambiguity values $I_{l,n}(m_a)$ of the sub-images. The phase of the ambiguity value $I_i(m_a)$ of each two channels is opposite, as shown in Fig.5. When the reconstructed imaging results of each channel are accumulated, the ambiguity is suppressed.

The conventional reconstruction method first reconstructs the echo data, and then uses the frequency domain imaging algorithm to process the reconstructed data. However, when the platform trajectory is curved, the phase cannot be accurately compensated, which invalidates the conventional reconstruction methods. As the proposed image domain reconstruction algorithm combines the reconstruction and the back projection strategy, it can solve this problem. The phase of each pixel value is accurately compensated during sub-image imaging by using the back projection algorithm shown in (17). Since the multichannel imaging result is the sum of the sub-images, the phase of each pixel in the final imaging result is also accurately compensated. So IDR can be applied to curved trajectory SAR reconstruction.

IV. EXPERIMENTAL RESULTS

In this section, the experimental results of the simulated and artificial multichannel data are presented, and the

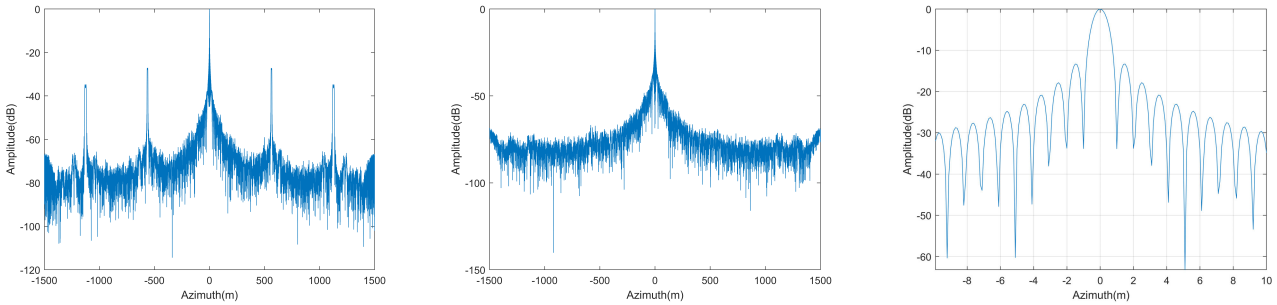

FIGURE 6. Imaging result in azimuth of the point target. (a) Without reconstruction. (b) The whole scene by by IDR reconstruction. (c) The scene center by IDR reconstruction.

performance is analyzed to validate the effectiveness of the proposed method described in section III.

A. SIMULATED MULTICHANNEL SAR DATA EXPERIMENT

The unambiguous reconstruction method proposed in this paper is applicable to multiple platforms, such as space-borne SAR, air-borne SAR, and the near-space hypersonic aircraft. Since an increasing research attention in the hypersonic aircraft [29], its system parameters are set as the reference for the latter simulation, shown in Table 1.

TABLE 1. Simulation parameters.

Parameters	value
Carrier frequency	10 GHz
Signal bandwidth	150 MHz
Sampling rata	210 MHz
PRF	700 Hz
Platform velocity	1900 m/s
Platform height	20 Km
Range	100 Km
Synthetic aperture length	1.53 Km
Channel number	4
The antenna spacing	1 m

This multichannel SAR system does not satisfy the uniform sampling condition. The antenna distribution is shown in Fig.2. According to the multichannel sampling model, described in section II, the effective phase centers (EPCs) of each channel can be obtained. The kth nonuniform sampling time $t_{k,n}$ for channel n corresponding to the EPCs can be expressed in (8). Aiming to better observe the ambiguity component in azimuth, one point target is simulated. According to (2), the point target echo data after range compression for each channel can be obtained as $s_r\left(\tau, t_{k,n}\right)$, where n=1, 2, 3, 4.

The raw data combined with four channels can be processed by the back projection (BP) algorithm. Fig.6(a) shows the azimuth imaging result of the point target without reconstruction. In this figure, it is obvious that the imagery suffers from residual azimuth ambiguities. The energy of ambiguities is around -30dB, causing multiple false targets in the final result. Besides, the minor targets will be submerged if distributed target exists. To solve the problem of unambiguous reconstruction, the proposed image domain reconstruction (IDR) approach is applied to the multichannel nonuniform sampling data. The reconstructed result by using IDR is depicted in Fig.6(b) and Fig.6(c), which show that the ambiguities can be suppressed well and the point target can be imaged. The amplitude of ambiguity is around -80dB as the background noise.

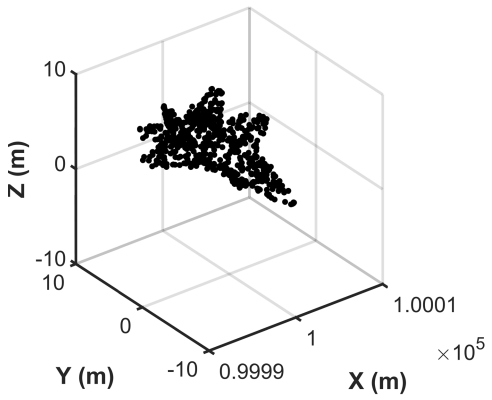

FIGURE 7. The airplane target model.

An airplane model constituted by several point scatters is simulated in the experiments to illustrate the effectiveness of the proposed method for the complex targets. Fig.7 depicts the airplane model. The length and width of the simulated airplane are 19m and 14m, respectively. Fig.8 shows the imaging results of this airplane by using BP without reconstruction and IDR respectively. The size of the imaging scene is 3000m*50m. Clearly, the result of BP without reconstruction suffers from the ambiguities, while IDR can suppress them well.

B. ARTIFICIAL MULTICHANNEL DATA EXPERIMENT

To further verify the proposed algorithm, artificial multichannel data, which is generated from an existing single-channel airborne SAR data, is used for this experiment. This single-channel data is collected by a high resolution SAR

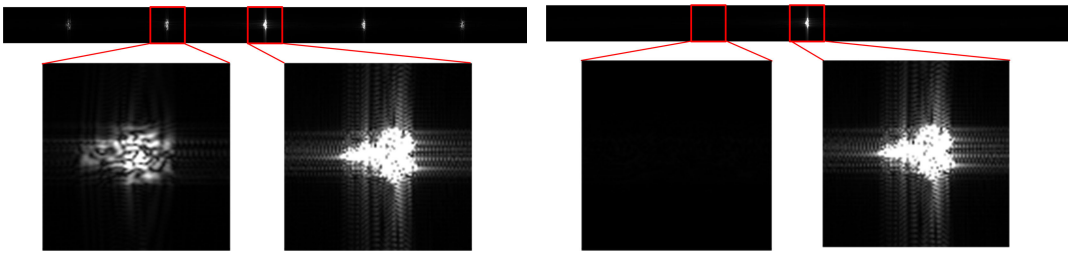

FIGURE 8. Imaging results of the airplane model. (a) Without reconstruction. (b) Reconstruction by IDR.

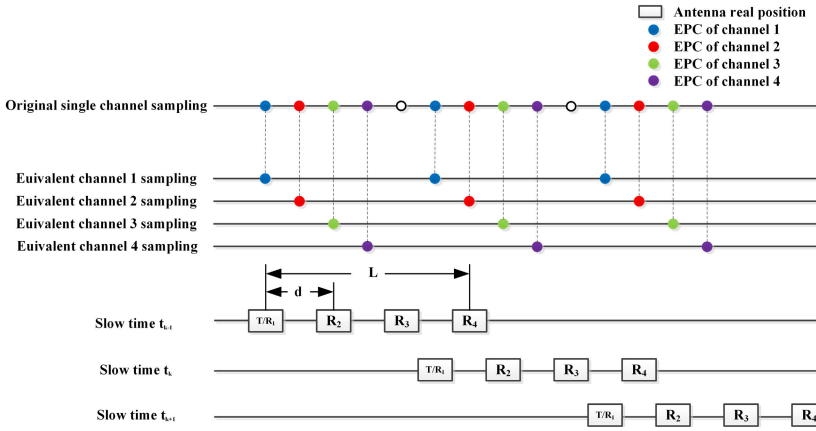

FIGURE 9. Resampling model of the equivalent four-channel SAR system for experimental data.

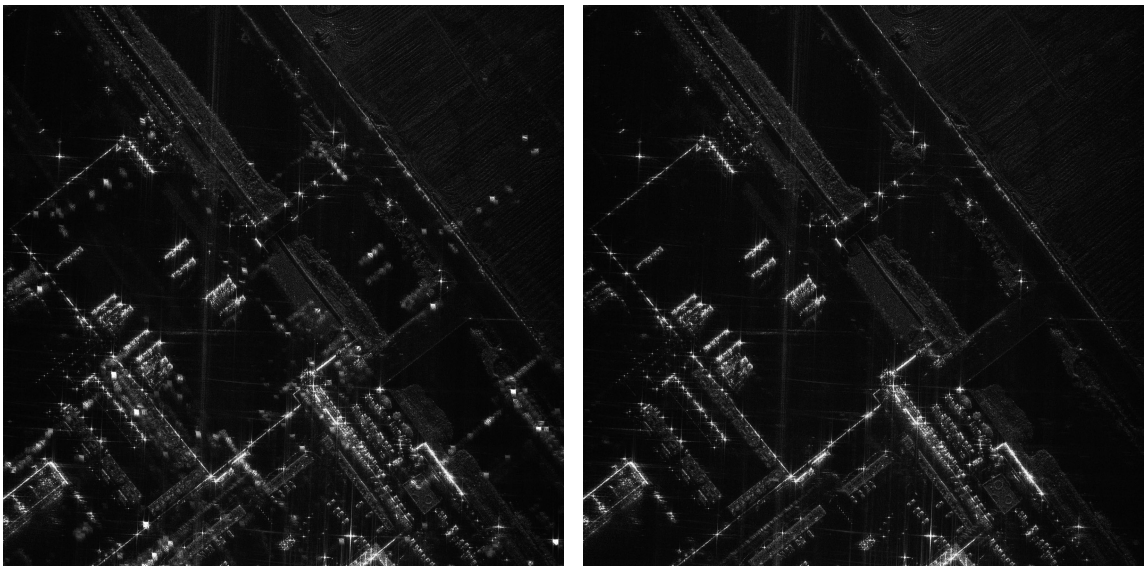

FIGURE 10. Imaging results of the equivalent multichannel SAR system raw data. (a) Without reconstruction. (b) Reconstruction by IDR.

system, operating in stripmap mode. The main parameters of this experimental radar are shown in Table 2.

To obtain equivalent four-channel periodic nonuniform sampling raw data, the single-channel uniform sampling raw data is resampled. Fig.9 shows the resampling model. The time of the five adjacent sampling points is used as the sampling period of the equivalent multichannel system. Since the original single-channel PRF is 2500Hz, the equivalent

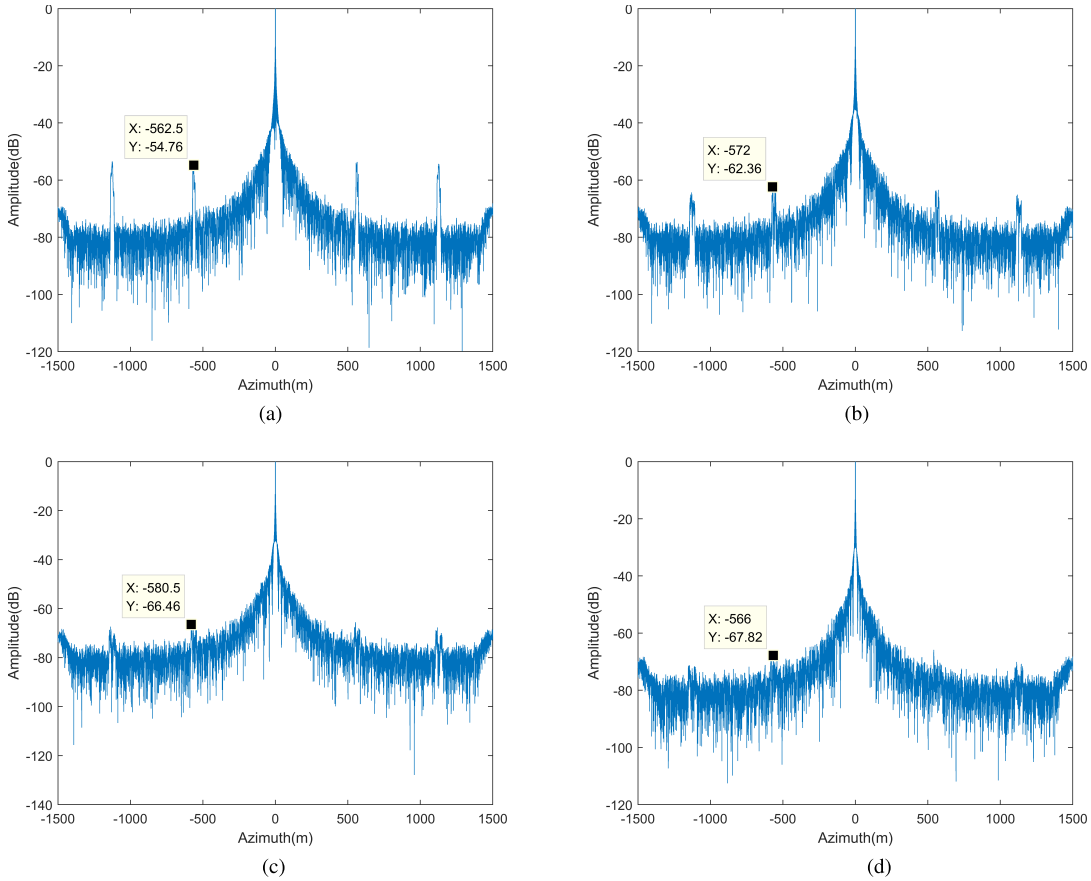

FIGURE 11. Imaging result with different interpolation period. (a) $L = 2$. (b) $L = 6$. (c) $L = 10$. (d) $L = 14$.

TABLE 2. Experimental parameters.

Parameters	value
Carrier frequency	35 GHz
Signal bandwidth	900 MHz
Range resolution	0.17m
Azimuth resolution	0.09m
PRF	2500 Hz
Platform velocity	60 m/s
Platform height	1 Km
Range	2.7 Km
Channel number	1

multichannel PRF is 500Hz. For every five adjacent sampling points, the first four sampling points correspond to the sampling points of channel 1, channel 2, channel 3, and channel 4, respectively. According to the sampling model, it is equivalent to the period nonuniform sampling of a four-channel SAR system shown in Fig.9. It has one transmitter and four receivers. This artificial data can completely equal to the real multichannel SAR data. If there are inconsistencies between the multiple channels, after the calibration of the channel phase errors, it will be the same as the data we get here [11].

The imaging results of the equivalent multichannel SAR system's raw data are shown in Fig.10. It is obvious that imaging result without reconstruction suffers from serious azimuth ambiguity, which is shown in Fig.10(a). Fig.10(b) is the imaging result by using the proposed method IDR. We can see that the ambiguity can be suppressed well. Consequently, the feasibility and effectiveness of the proposed unambiguous reconstruction method IDR are verified by the processing results of the equivalent multichannel SAR data.

Moreover, to compare the computational complexity of different methods, the running times of each step of IRA and the IDR are measured, which are shown in Table 3.

TABLE 3. Comparison of runtime.

Methods	Steps	Runtime	Total time
IRA	Raw data reconstruction Imaging	92s 15s	107s
IDR	Calculating interpolation coefficient Generating sub-images Fusing sub-images	0.2s 306s 7s	313.2s
Update IDR	Calculating interpolation coefficient Fusing sub-images	0.2s 7s	7.2s

The algorithms run on the following hardware: Intel i7 6700 CPU, 2080Ti GPU. Here, the IRA method uses the

BP algorithm for imaging, and the IDR uses the back projection principle to generate the sub-images. In BP imaging, GPU parallel processing is used to improve imaging efficiency [30]. The main runtime of IDR is generating sub-images, which is more than the traditional reconstruction methods. But when updating the reconstruction results, the traditional method needs to reconstruct the echo again in the raw data domain, and then use this echo for imaging. Updating IDR only needs to calculate the interpolation coefficients and use the previous sub-images for fusion, whose runtime is very small. Besides, it does not need to generate the sub-images again, which greatly reduces the amount of calculation.

C. INTERPOLATION PERIOD ANALYSIS

To evaluate the effect of the interpolation period on the performance of the proposed algorithm, the reconstruction results of the point target described in section IV-A with different interpolation period are analyzed. The reconstruction results are shown in Fig.11. The results show that the larger the interpolation period, the better the performance of the azimuth ambiguity suppression. When the interpolation period is more than 6, the ambiguity value is less than -60dB. Let the imaging scene's size be 50m * 100m. The reconstruction time with different interpolation period is shown in Fig.12. The reconstruction time increases linearly. This is because the larger the interpolation period, the more data needs to be used for interpolation, consuming more processing time. The larger the interpolation period used for reconstruction, the better the ambiguity can be suppressed. However, a larger interpolation period means more sub-images need to be interpolated, which will consume more time. Moreover, as the interpolation coefficient is similar to the *sinc* function, an excessively enlarging interpolation period has little effect on improving the quality of the reconstructed image. Considering the reconstruction accuracy and efficiency, it is reasonable to set the interpolation period to 6.

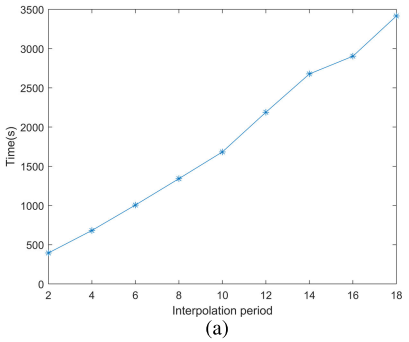

FIGURE 12. The reconstruction time with different interpolation periods.

D. UNAMBIGUOUS RECONSTRUCTION FOR CURVED TRAJECTORY

The curved motion trajectory of the flying platform results in serious range migration, which brings challenges to the unambiguous reconstruction. To analyze the performance of the proposed method for the curved trajectory, IDR is applied to the simulated curved trajectory data. The geometric model is shown in Fig.13. Due to the curved trajectory, the instantaneous speed of the platform increases. The bandwidth of the azimuth echo signal with the curved trajectory is greater than that with the linear trajectory. Multichannel equivalent azimuth sampling rate needs to be larger than the bandwidth of the azimuth signal. Thus, let the PRF of the SAR system be 1000Hz. According to the PRF, the antenna spacing that meets the uniform sampling condition is $0.95m$. Let the simulated antenna spacing be $0.8m$, which makes the system form non-uniform sampled. The other parameters are the same as the simulation for linear flight trajectory shown in Tab.1. The curved trajectory is shown in Fig.14. It only deviates in height direction compared with the linear trajectory, which has a greater impact on imaging. Since the multichannel antennas

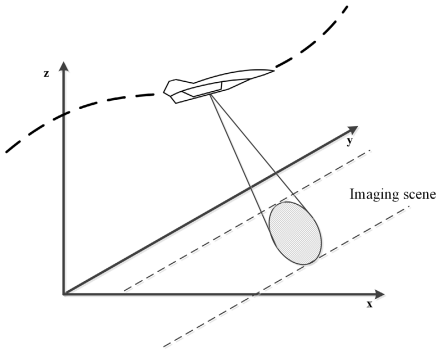

FIGURE 13. The geometric model for the curved trajectory.

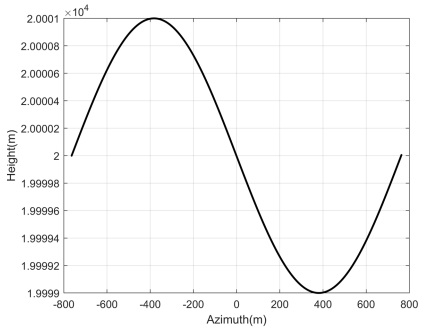

FIGURE 14. The curved trajectory of the moving platform.

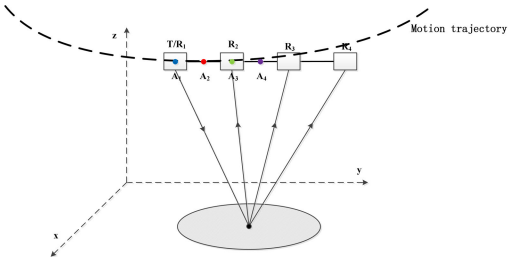

FIGURE 15. The EPC distribution on the curved trajectory.

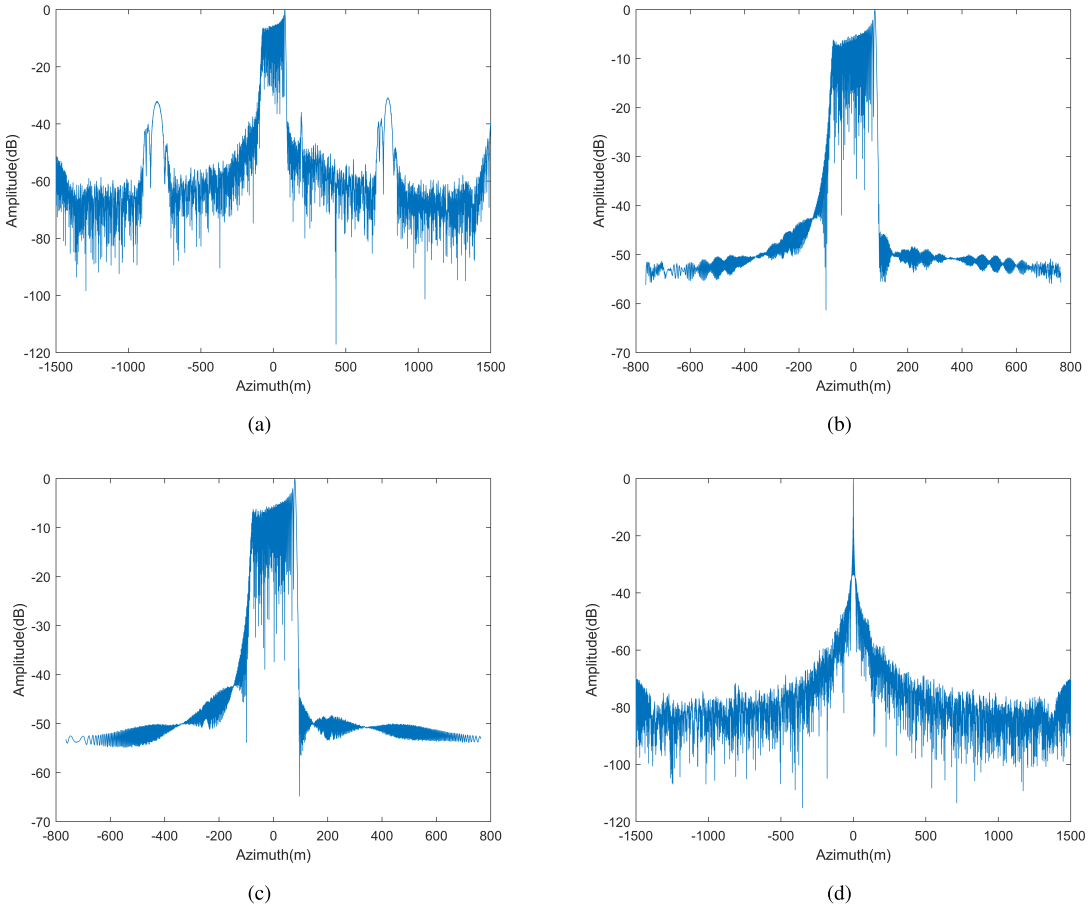

FIGURE 16. Imaging results for the curved trajectory. (a) Without reconstruction. (b) Reconstruction by the IRA. (c) Reconstruction by SRA. (d) Reconstruction by IDR.

are linearly distributed on the platform, all EPCs cannot be distributed on the curved trajectory, which is displayed in Fig.15. Generally, as the curvature of the curved trajectory is small, that is, the instantaneous turning radius of the flight platform is large, EPCs can be approximately distributed on the curved trajectory.

The imaging results in azimuth before reconstruction without phase compensation are shown in Fig.16 (a). The reconstruction results are shown in Fig.16 (b), (c), and (d) using the interpolation reconstruction algorithm (IRA), the spectrum reconstruction algorithm (SRA) and the proposed image domain reconstruction method (IDR), respectively. These conventional methods perform the reconstruction in the raw data domain and then use a frequency-domain imaging algorithm for SAR imaging. It is difficult to adapt to the curved trajectory SAR reconstruction. Compared with conventional methods, the results demonstrate that the proposed algorithm can effectively suppress the ambiguity and obtain a well-focused image for the curved trajectory SAR. If we directly combine the traditional method and the BP algorithm, the reconstruction quality is the same as IDR, but there are still disadvantages that it is difficult to update the reconstruction result.

To further evaluate the performance of IRA, SRA, and IDR, some metrics which consist of the image entropy and contrast are measured and compared. The entropy can be expressed as

$$\begin{aligned}\varepsilon(\Psi) &= \sum_{m=1}^{M} \frac{|I_\Psi(m)|^2}{S} \ln \frac{S}{|I_\Psi(m)|^2} \\ &= \ln S - \frac{1}{S} \sum_{m=1}^{M} |I_\Psi(m)|^2 \ln |I_\Psi(m)|^2 \end{aligned} \tag{20}$$

where,

$$S = \sum_{m=1}^{M} |I_\Psi(m)|^2 \tag{21}$$

The image contrast is defined as

$$Contrast = \frac{\sqrt{\sum_{m=1}^{M} (P(m) - u_{P(m)})^2 / M}}{u_{P(m)}} \tag{22}$$

where $I_{\Psi(m)}$ is the pixel value of the image, $P(m)$ is the image pixels intensity, $u_{P(m)}$ is the mean of the intensity,

m is the sequence number of the pixels, M is the number of the image pixels. Generally, a much more focused image brings in higher image quality with lower entropy and higher contrast.

The measured entropy and contrast of Fig.16 are displayed in Table 4. The results show that the image reconstructed by IDR has around three times larger contrast value and two times less entropy value compared with the conventional reconstruction methods. It further demonstrates that the IDR has its superiority for the cured trajectory situation in contrast with those traditional ones.

TABLE 4. The comparison of imaging quality metrics for the curved trajectory.

Methods	Entropy	Contrast
Without reconstruction	7.36	27.63
IRA	7.03	78.27
FRA	7.03	77.95
IDR	3.05	253.30

The proposed method can calculate the phase history between the pixels of the imaging scene and the platform at each slow time when the sub-images are obtained. So it can accurately compensate the phase error corresponding to the curved trajectory. Compared with other reconstruction algorithms, no additional phase compensation is needed for curved trajectories.

V. CONCLUSION

In this paper, for the multichannel nonuniform sampling signal, a novel unambiguous reconstruction method is proposed from the viewpoint of image domain processing. According to the multichannel sampling model, BP algorithm is first employed for SAR imaging to get the sub-images. Then, the image domain reconstruction is executed by the weighted fusing of the sub-images through the interpolation coefficient. This method integrates the reconstruction into the multichannel imaging process and expresses the reconstruction as image fusion, simplifying the reconstruction process. As the proposed method separates the interpolation coefficient that is independent of the sub-images, it is convenient for adjusting the reconstruction result. The method can implement the update by re-calculating the correct interpolation coefficient and fusing the sub-images, whose computation amount is small. Moreover, because of the combination of the reconstruction and the back projection approach, the phase of each pixel value in the sub-image imaging is accurately compensated. Thus, the proposed method performs well for the curved SAR reconstruction processing. In addition, an appropriate interpolation period, which affects the reconstruction image quality and efficiency, is analyzed and obtained. Finally, both the simulation results and the equivalent multichannel data generated from an existing SAR system verifies the method effectiveness.

REFERENCES

[1] T. Yang, Y. Wang, and W. Li, "A moving target imaging algorithm for HRWS SAR/GMTI systems," *IEEE Trans. Aerosp. Electron. Syst.*, vol. 53, no. 3, pp. 1147–1157, Jun. 2017.
[2] N. Sakar, M. Rodriguez-Cassola, P. Prats–Iraola, A. Reigber, and A. Moreira, "Investigations on the reconstruction of multistatic large along-track sar constellations for hrws imaging," in *Proc. IEEE Int. Geosci. Remote Sens. Symp. IGARSS*, Jul. 2018, pp. 3659–3662.
[3] D. Wu, Y. Zhang, D. Zhu, S. Wang, and M. Shen, "A channel calibration algorithm based on isolated scatterers for multi-channel HRWS-SAR," *IEEE Access*, vol. 7, pp. 135665–135677, 2019.
[4] H. Wang, Y. Zhang, J. Xu, G. Liao, and C. Zeng, "A novel range ambiguity resolving approach for high-resolution and wide-swath SAR imaging utilizing space-pulse phase coding," *Signal Process.*, vol. 168, Mar. 2020, Art. no. 107323.
[5] G. Krieger, N. Gebert, and A. Moreira, "Unambiguous SAR signal reconstruction from nonuniform displaced phase center sampling," *IEEE Geosci. Remote Sens. Lett.*, vol. 1, no. 4, pp. 260–264, Oct. 2004.
[6] N. Gebert, G. Krieger, and A. Moreira, "Digital beamforming on receive: Techniques and optimization strategies for high-resolution wide-swath SAR imaging," *IEEE Trans. Aerosp. Electron. Syst.*, vol. 45, no. 2, pp. 564–592, Apr. 2009.
[7] Z. Li, H. Wang, T. Su, and Z. Bao, "Generation of wide-swath and high-resolution SAR images from multichannel small spaceborne SAR systems," *IEEE Geosci. Remote Sens. Lett.*, vol. 2, no. 1, pp. 82–86, Jan. 2005.
[8] S.-X. Zhang, J.-L. Sheng, and M.-D. Xing, "A novel focus approach for squint mode multi-channel in azimuth high-resolution and wide-swath SAR imaging processing," *IEEE Access*, vol. 6, pp. 74303–74319, 2018.
[9] S.-X. Zhang, S. Li, Y. Liu, M.-D. Xing, and J. Chen, "A novel azimuth Doppler signal reconstruction approach for the GEO-LEO bi-static multi-channel HRWS SAR system," *IEEE Access*, vol. 7, pp. 39539–39546, 2019.
[10] N. Gebert, G. Krieger, and A. Moreira, "Multichannel azimuth processing in ScanSAR and TOPS mode operation," *IEEE Trans. Geosci. Remote Sens.*, vol. 48, no. 7, pp. 2994–3008, Jul. 2010.
[11] S. Zhao, R. Wang, Y. Deng, Z. Zhang, N. Li, L. Guo, and W. Wang, "Modifications on multichannel reconstruction algorithm for SAR processing based on periodic nonuniform sampling theory and nonuniform fast Fourier transform," *IEEE J. Sel. Topics Appl. Earth Observ. Remote Sens.*, vol. 8, no. 11, pp. 4998–5006, Nov. 2015.
[12] S.-X. Zhang, M.-D. Xing, X.-G. Xia, L. Zhang, R. Guo, Y. Liao, and Z. Bao, "Multichannel HRWS SAR imaging based on range-variant channel calibration and Multi-Doppler-Direction restriction ambiguity suppression," *IEEE Trans. Geosci. Remote Sens.*, vol. 52, no. 7, pp. 4306–4327, Jul. 2014.
[13] T. Yang, Z. Li, Z. Suo, Y. Liu, and Z. Bao, "Performance analysis for multichannel HRWS SAR systems based on STAP approach," *IEEE Geosci. Remote Sens. Lett.*, vol. 10, no. 6, pp. 1409–1413, Nov. 2013.
[14] Q. Chen, Y.-K. Deng, Y.-D. Liu, and X.-Q. Shang, "SAR azimuth signal reconstruction based on adaptive filtering for the DPC-MAB SAR system," *J. Electron. Inf. Technol.*, vol. 34, no. 6, pp. 1331–1336, Aug. 2012.
[15] I. Sikaneta, C. H. Gierull, and D. Cerutti-Maori, "Optimum signal processing for multichannel SAR: With application to high-resolution wide-swath imaging," *IEEE Trans. Geosci. Remote Sens.*, vol. 52, no. 10, pp. 6095–6109, Oct. 2014.
[16] L. Guangyan, W. Youlin, and L. Youquan, "Unambiguous reconstruction and imaging of nonuniform sampling SAR signals," in *Proc. 1st Asian Pacific Conf. Synth. Aperture Radar*, Nov. 2007, pp. 253–256.
[17] Z. Zong, "Study on waveform design and imaging technology for formation-flying satellites SAR," Ph.D. dissertation, School Inf. Commun. Eng., Univ. Electron. Sci. Technol. China, Chengdu, China, 2012.
[18] F.-F. Yang, W. Min, and D.-N. Liang, "Small satellite multi-channel sar unambiguous imaging based on nonuniform sampling," *Acta Electronica Sinica*, vol. 35, no. 9, pp. 1754–1756, 2007.
[19] Z. Zhu, Z. Zhang, and Y. Wang, "Fast algorithm for non-uniformly sampled signal spectrum reconstruction," *J. Electron.*, vol. 30, no. 3, pp. 231–236, Jun. 2013.
[20] Z. Zhu, Z. Zhang, R. Wang, and L. Guo, "Out-of-Band ambiguity analysis of nonuniformly sampled SAR signals," *IEEE Geosci. Remote Sens. Lett.*, vol. 11, no. 12, pp. 2027–2031, Dec. 2014.
[21] L. Qi, R. Tao, S. Zhou, and Y. Wang, "Detection and parameter estimation of multicomponent LFM signal based on the fractional Fourier transform," *Sci. China Ser. F, Inf. Sci.*, vol. 47, no. 2, p. 184, 2004.

[22] R. Tao, B.-Z. Li, and Y. Wang, "Spectral analysis and reconstruction for periodic nonuniformly sampled signals in fractional Fourier domain," *IEEE Trans. Signal Process.*, vol. 55, no. 7, pp. 3541–3547, Jul. 2007.
[23] J. Yen, "On nonuniform sampling of bandwidth-limited signals," *IRE Trans. Circuit Theory*, vol. 3, no. 4, pp. 251–257, Dec. 1956.
[24] M. D. Desai and W. K. Jenkins, "Convolution backprojection image reconstruction for spotlight mode synthetic aperture radar," *IEEE Trans. Image Process.*, vol. 1, no. 4, pp. 505–517, Oct. 1992.
[25] A. W. Doerry, E. E. Bishop, and J. A. Miller, "Basics of backprojection algorithm for processing synthetic aperture radar images," Sandia Nat. Laboratories, Albuquerque, NM, USA, Tech. Rep. SAND2016–1682, 2016.
[26] F. C. Peyrin, "The generalized back projection theorem for cone beam reconstruction," *IEEE Trans. Nucl. Sci.*, vol. NS-32, no. 4, pp. 1512–1519, Aug. 1985.
[27] S. Jun, Z. Xiaoling, Y. Jianyu, and W. Chen, "APC trajectory design for 'One-Active' linear-array three-dimensional imaging SAR," *IEEE Trans. Geosci. Remote Sens.*, vol. 48, no. 3, pp. 1470–1486, Mar. 2010.
[28] L. Zhang, M.-D. Xing, C.-W. Qiu, and Z. Bao, "Adaptive two-step calibration for high-resolution and wide-swath SAR imaging," *IET Radar, Sonar Navigat.*, vol. 4, no. 4, p. 548, Aug. 2010.
[29] R. Zhou, J. Sun, Y. Hu, and Y. Qi, "Multichannel high resolution wide swath SAR imaging for hypersonic air vehicle with curved trajectory," *Sensors*, vol. 18, no. 2, p. 411, 2018.
[30] F. Ahmed and H. Timothy, "GPU-accelerated synthetic aperture radar backprojection in cuda," in *Proc. IEEE Radar Conf.*, May 2010, pp. 1408–1413.

LIMING ZHOU received the B.Sc. degree in optoelectronic engineering from the University of Electronic Science and Technology of China (UESTC), Chengdu, China, in 2015, where he is currently pursuing the Ph.D. degree in signal and information processing.

His research interests include radar signal processing and multi-channel synthetic aperture radar systems.

XIAOLING ZHANG (Member, IEEE) received the B.S., M.Sc., and Ph.D. degrees in electronic engineering from the University of Electronic Science and Technology of China (UESTC), Chengdu, China, in 1985, 1988, and 2000, respectively.

She joined UESTC, in 2000, where she is currently a Professor. Her research interests include radar signal processing and classification/recognition.

YANGYANG WANG received the M.S. degree from the University of Electronic Science and Technology of China (UESTC), Chengdu, China, in 2018, where he is currently pursuing the Ph.D. degree with a focus on synthetic aperture radar (SAR) imaging and motion compensation.

His current research interests include SAR imaging and sparse signal processing.

LIANG LI received the B.S. degree from the School of Computer and Communication Engineering, Northeastern University at Qinhuangdao, Qinhuangdao, China, in 2016. He is currently pursuing the Ph.D. degree in signal and information processing with the University of Electronic Science and Technology of China (UESTC). His research interests include radar signal processing, SAR systems, and RCS measurements.

LIMING PU received the B.S. degree from the Nanjing University of Science and Technology, in 2016. He is currently pursuing the Ph.D. degree in signal and information processing with the University of Electronic Science and Technology of China, Chengdu, China.

His research interests include synthetic aperture radar imaging processing and interferometric synthetic aperture radar (InSAR) processing.

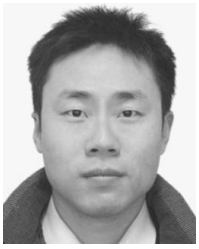

JUN SHI (Member, IEEE) received the B.S., M.Sc., and Ph.D. degrees in electronic engineering from the University of Electronic Science and Technology of China (UESTC), Chengdu, China, in 2002, 2005, and 2009, respectively.

He joined UESTC, in 2009, where he is currently an Associate Professor. His research interests include radar signal processing and synthetic aperture radar systems.

SHUNJUN WEI (Member, IEEE) received the B.S., M.Sc., and Ph.D. degrees in electronic engineering from the University of Electronic Science and Technology of China (UESTC), Chengdu, China, in 2006, 2009, and 2013, respectively.

He joined UESTC, in 2014, where he is currently an Associate Professor. His research interests include radar signal processing and synthetic aperture radar systems.